View Article Online
DOI: 10.1039/C7TB03200E

Journal of Materials Chemistry B

PAPER

Imaging and evaluation of sulfane sulfur in acute brain ischemia using a mitochondria-targeted near-infrared fluorescent probe

Received 00th January 20xx,
Accepted 00th January 20xx

DOI: 10.1039/x0xx00000x

www.rsc.org/

Min Gao,[ac] Rui Wang,[a] Fabiao Yu,[ab]* Jinmao You,[b] Lingxin Chen[ab]*

Ischemia is a pathological condition owing to the deficiency of blood supply to a limited area of tissue. Ischemia can induce burst production of reactive oxygen species and lead to oxidative damage. As a family member of reactive sulfur species, sulfane sulfur plays important physiological roles in many biological events including synthesis of cofactors, modulation of enzyme activities, sulfuration of *t*RNA, and especially regulating the intracellular redox state. We hypothesize that the endogenous level of sulfane sulfur will be adjusted to deal with ischemia-induced oxidative damage. Therefore, the bioimaging of sulfane sulfur real-time changes during ischemia is important for better understanding its physiological processes. Herein, we describe the development of a mitochondria-targeted fluorescent probe Mito-SH that allowed for selective and sensitive detection of sulfane sulfur. Mito-SH is designed on the basis of the tautomerization of sulfane sulfur to thiosulfoxide, which ensures its high selectivity and sensitivity. A lipophilic triphenylphosphonium cation is selected as the mitochondria-targeted moiety, which can precisely navigate Mito-SH into mitochondria. The emission profile of *azo*-BODIPY fluorophore locates at near-infrared region, which deeply penetrates tissue and effectively avoids the interference of biological background. Mito-SH exhibits the desirable combination of selectivity, sensitivity and excellent fluorescence response upon reaction with sulfane sulfur in cells. By employing Mito-SH, we evaluate the real-time sulfane sulfur dynamic changes under oxygen-glucose deprivation. Finally, Mito-SH has been successfully used for imaging sulfane sulfur changes caused by acute ischemia in mice.

Introduction

Cells require continuous assimilation of oxygen and glucose to maintain adequate energy supply. Ischemia is a pathological condition which is limited blood supply to an area of tissue and then lead to cellular hypoxia. The deficiency in blood supply can affect the expression of many proteins, which may cause destruction in the ischemic tissue. Accumulating evidences indicate that the ischemia-induced injury results from the burst production of reactive oxygen species (ROS). Oxidative damage is always in checking by antioxidant defense systems, but an excessive amount of ROS will cause irreparable damage, which contributes to several pathological conditions including aging, carcinogenesis, and stroke.[1] Reactive sulfur species (RSS) which hold antioxidant and cytoprotection properties belongs to antioxidant regulatory systems. As a family member of RSS, sulfane sulfur functions in many important physiological processes, including synthesis of cofactors, modulation of enzyme activities, sulfuration of tRNA, and especially regulation of redox state.[2, 3] Once ischemia occurs, the level of sulfane sulfur will be adjusted to deal with the ROS generation. That is, the overall sulfane sulfur may indicate the physiological and pathological status of the organism. Therefore, the real-time bioimaging of dynamic changes of sulfane sulfur during ischemia can facilitate to better understanding physiological processes.

Sulfane sulfur which contains sulfur in the thiosulfoxide form (represented as S^0) includes persulfides (R–S–SH), hydrogen polysulfides (H_2S_n, n ≥ 1), polysulfides (R–S–S_n–S–R, n ≥ 1), and protein-bound elemental sulfur (S_8). Cystathionine *β*-synthase (CBS), cystathionine *γ*-lyase (CSE) and 3-mercaptopyruvate sulfurtransferase (3-MST) which have been consider to produce H_2S are now involved in the generation of sulfane sulfur.[4] It is worth noting that sulfane sulfur also can be generated through non-enzyme way that endogenous H_2S upon direct reaction with ROS. In addition, sulfane sulfur exhibits more reactive than H_2S in many physiological processes. It can regulate the activities of ion channels and a tumor suppressor, which may the actual signaling molecules in cell signal transduction.[5-12] Moreover, sulfane sulfur exists in plants of the genus *Allium* in nature. These vegetables which contain sulfane sulfur derivatives have attracted considerable interest ranging from redox signalling to health-related effects.[13] Therefore, the potential biochemical impact of

[a] Key Laboratory of Coastal Environmental Processes and Ecological Remediation, Research Centre for Coastal Environmental Engineering and Technology, Yantai Institute of Coastal Zone Research, Chinese Academy of Sciences, Yantai 264003, China. *E-mail: fbyu@yic.ac.cn, lxchen@yic.ac.cn
[b] Key Laboratory of Life-Organic Analysis, Key Laboratory of Pharmaceutical Intermediates and Analysis of Natural Medicine, College of Chemistry and Chemical Engineering, Qufu Normal University, Qufu 273165, China.
[c] University of Chinese Academy of Sciences, Beijing 100049, China.
Electronic Supplementary Information (ESI) available: details and more information of experiments. See DOI: 10.1039/x0xx00000x

Published on 05 February 2018. Downloaded by Fudan University on 06/02/2018 00:55:19.

Journal of Materials Chemistry B Accepted Manuscript

Please do not adjust margins

View Article Online
DOI: 10.1039/C7TB03200E

Published on 05 February 2018. Downloaded by Fudan University on 06/02/2018 00:55:19.

sulfane sulfur provides an innovative way for development of novel therapeutic drugs.[14]

Sulfane sulfur which contains high reactive sulfur atom in the thiosulfoxide form (represented as S^0) has the unique ability to covalently bind to another sulfur atom. Sulfane sulfur exhibits high electrophilic property, and it can react with nucleophiles. Thus, the previous method for detection of sulfane sulfur is reacting with cyanide ions (CN^-) to form thiocyanate (SCN^-), and then it can be measured as ferric thiocyanate.[15] However, this method requires extensive sample processing. It cannot meet the demands of *in situ* detection by sensitivity and selectivity. As the increasing recognition of the significance of sulfane sulfur, the more suitable approach for real-time detect intracellular sulfane sulfur need to be developed.[16] Fluorescent probes offer an appealing approach to real time imaging reactive small molecules in living cells for achieving *in situ* detection.[17-24] Xian's and Hanaoka's groups have made efforts to develop series of fluorescent probes such as SSP and SSip-1 for sulfane sulfur detection in living cells.[25, 26] Most of other fluorescent probes are designed for detection of a sub-derivative of sulfane sulfur, hydrogen polysulfides (H_2S_n).[27-35] Recently, our group focuses on the investigation of the cross-talk between H_2S_n and superoxide anion in living cells using near-infrared (NIR) fluorescent probes.[36, 37] We also report a ratio fluorescent probe for the detection of hydropersulfide (Cys-SSH, another derivative of sulfane sulfur) in living cells and in tumor-bearing mice.[38] The new generation of fluorescent probe for sulfane sulfur detection should meet two additional requirements: i) The probes whose excitation and emission lie in NIR region allow for *in vivo* imaging due to their deep tissue penetration and minimal interference from background autofluorescence.[39-41] ii) The probes should possess the mitochondria-targeting ability due to 60% sulfane sulfur is associated with mitochondria. Mitochondria which is crucial for maintain cell redox milieu is the energy supply of cells, where is the main place that undertakes the generation of ROS.[42]

Herein, we introduced a new fluorescent probe Mito-SH that enabled ones to monitor the production of sulfane sulfur in living cells, in tissues, and *in vivo*. The probe Mito-SH was composed of three moieties: an *azo*-BODIPY as NIR fluorophore, a thiophenol group as response unit, and lipophilic triphenylphosphonium cation as mitochondria-targeted group. The probe had been used to image sulfane sulfur in living cells and detect the level changes of sulfane sulfur during oxygen-glucose deprivation process. We also assessed physiological functions of sulfane sulfur in the hippocampus of acute ischemia mice models.

Results and discussion

Molecular design of Mito-SH for sulfane sulfur

As shown in Scheme 1, the tautomerization of sulfane sulfur to thiosulfoxide can generate a reactive sulfur atom that has electrophilic property and it can react with nucleophiles. Therefore, sulfane sulfur can transfer this sulfur atom to other RSS forming hydropersulfides (R-S-SH) and polysulfides (-S-S_n-S-). Taking advantage of this reactive property, the mercapto (-SH) in thiophenol group has been proved to be a suitable candidate for capturing sulfane sulfur.[25] However, the fluorescence excitation and emission locating in the UV or visible region can interfere by biological autofluorescence. And the tissue penetration will severely limit the *in vivo* application. Therefore, it is necessary to develop a fluorescent probe that has NIR absorption and emission profiles for overall sulfane sulfur detection *in vivo*.[43] Herein, we conceived a probe Mito-SH with a NIR azo-BODIPY fluorophore. The structure and proposed reaction mechanism was illustrated in Scheme 1. The reactive sulfur atom of thiosulfoxide firstly attached with -SH in Mito-SH to form an unstable intermediate persulfide (R-SSH). Subsequently, the intermediate underwent intramolecular nucleophilic attacking on the ester moiety and carrying out an intramolecular cyclization to release the fluorophore, which triggered the fluorescence emission. To selectively detect mitochondria sulfane sulfur, the lipophilic triphenylphosphonium cation was introduced as the mitochondria-targeted carrier.

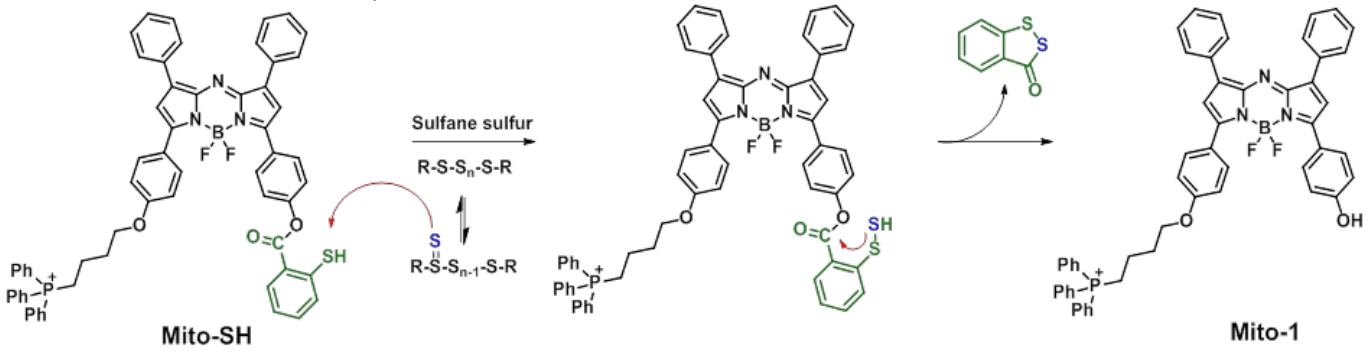

Scheme 1 Structure of Mito-SH and proposed mechanism of Mito-SH for the detection of sulfane sulfur.

Journal of Materials Chemistry B Accepted Manuscript

This journal is © The Royal Society of Chemistry 20xx

Please do not adjust margins

View Article Online
DOI: 10.1039/C7TB03200E

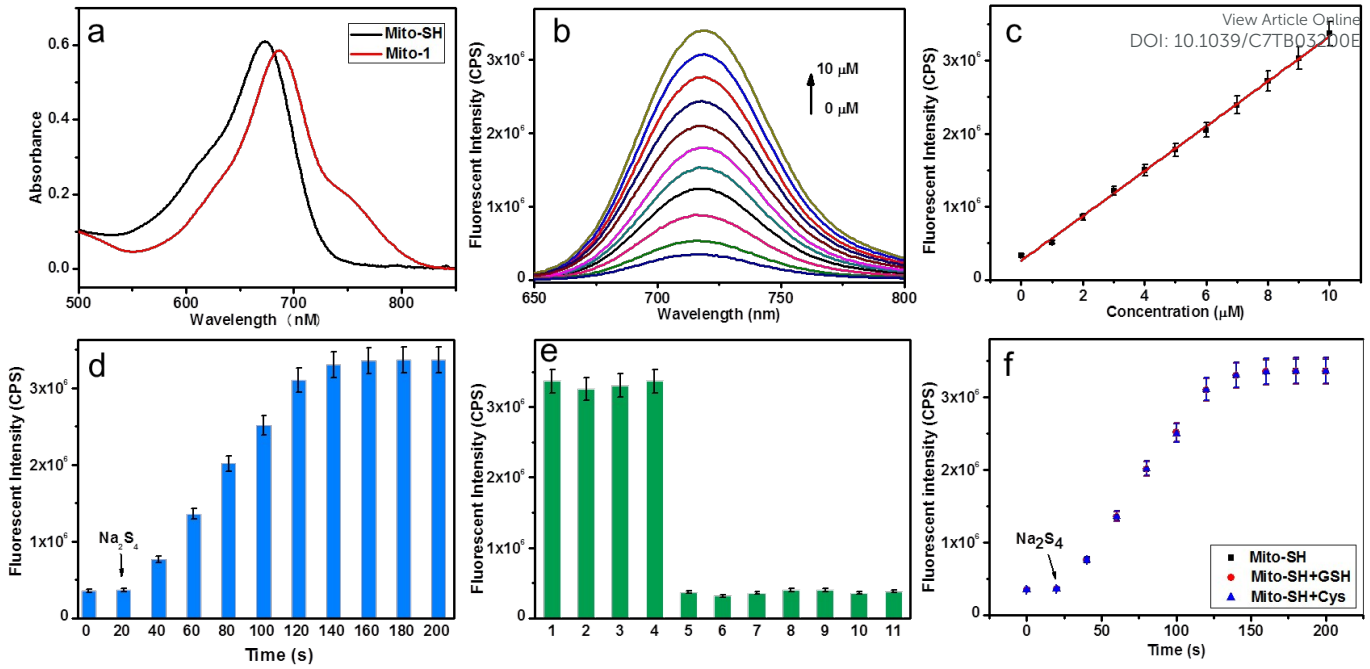

Fig. 1 Absorption (a) and fluorescence (b) spectra of Mito-SH (10 μM) upon addition of Na_2S_4 (0 - 10 μM). (c) The linear relationship between the fluorescence intensity and the concentration of Na_2S_4. (d) Time-dependent changes in the fluorescence intensity of Mito-SH (10 μM) in the presence of Na_2S_4 (10 μM). (e) Fluorescence response of 10 μM Mito-SH to biologically relevant RSS. Bars represent relative responses at 737 nm after addition of RSS. Legend: 1. 10 μM Na_2S_4; 2. 10 μM Na_2S_4; 3. 10 μM S_8; 4. 10 μM Cys–polysulfide; 5. 100 μM Cystine; 6. 100 μM GSSG; 7. 1 mM Cysteine; 8. 1 mM GSH; 9. 1 mM Hcy; 10. 1 mM NaHS; 11. 100 μM L-cysteine methyl ester. (f) Time-dependent fluorescence changes of Mito-SH upon addition of Na_2S_4 (10 μM) in the presence of interfering thiol GSH (1 mM) and H_2S (1 mM). Data were acquired in 10 mM HEPES buffered at pH 7.4 (0.5% DMSO, 0.4% Tween 80). λ_{ex} = 688 nm, λ_{em} = 737 nm.

Spectral properties of Mito-SH

The optical properties of Mito-SH towards sulfane sulfur were examined under simulated physiological conditions (10 mM HEPES buffer, pH 7.4, 0.5% DMSO, 0.4% Tween 80). As shown in Fig. 1a, a strong absorption band of Mito-SH centered at 679 nm and a new absorption maximum of Mito-1 emerged at 688 with a slight red shift upon addition of Na_2S_4 in absorption spectra. Upon reacted with Na_2S_4, Mito-SH brought a remarkable fluorescence enhancement at 723 nm (Fig. 1b). In a fluorimetric titration study, the fluorescence intensity of Mito-SH increased linearly as the concentrations of Na_2S_4 changed from 0 to 10 μM at 723 nm (Fig. 1c). The regression equation was $F_{\lambda ex/em(679/723\ nm)} = 3.06 \times 10^5\ [Na_2S_4] + 2.66 \times 10^5$ with a linear fitting constant r = 0.9992. The experimental detection limit was found to be 73 nM. The linear dependence of the triggered fluorescence intensity on Na_2S_4 was essential and important for the quantitative determination of Na_2S_4 concentrations. In addition, the maximum intensity was reached in 100 s with a 10-fold fluorescence enhancement, which suggested that the fluorescence turn-on reaction was efficiency and fast (Fig. 1d). The performance of Mito-SH and Mito-1 with different pH values ranging from 2.0 to 10.0 was performed. As shown in Fig. S1, Mito-SH showed a stable fluorescence at the range of pH 4.0 to 10.0 in a HEPES buffer solution. Mito-1 showed no significant fluorescent intensity changes from pH 4 to 7.8. These results showed that Mito-SH can be applied for detecting sulfane sulfur without interference of pH in the biological environment.

Selectivity

To test feasibility of Mito-SH as a sulfane sulfur-selective probe, we focused our attention on the selectivity of the newly synthesized Mito-SH across a panel of RSS. As illustrated in Fig. 1e, only the family members of sulfane sulfur, such as Na_2S_4, Na_2S_4, S_8, Cys–polysulfide, triggered a dramatic fluorescence change towards Mito-SH (10 μM). In contrast, the addition of other relevant species, including homocysteine (HCy), cysteine (Cys), cystine, glutathione (GSH), oxidized glutathione (GSSG) and NaHS, did not induce significantly fluorescence change of Mito-SH. Subsequently, the nucleophile, L-cysteine methyl ester also could not interfere fluorescence change of Mito-SH. The reactive dynamics of Mito-SH towards Na_2S_4 (10 μM) in the presence of physiological concentrations of GSH and H_2S further supported that Mito-SH possessed high selectivity for sulfane sulfur (Fig. 1f). Additionally, the reactive oxygen species (ROS) did not interfere fluorescence change of Mito-SH (Fig. S2). These results indicated that the structural motif of Mito-SH was considerably efficient in detecting sulfane sulfur over other relevant species in biological system.

Published on 05 February 2018. Downloaded by Fudan University on 06/02/2018 00:55:19.

Journal of Materials Chemistry B Accepted Manuscript

Please do not adjust margins

View Article Online
DOI: 10.1039/C7TB03200E

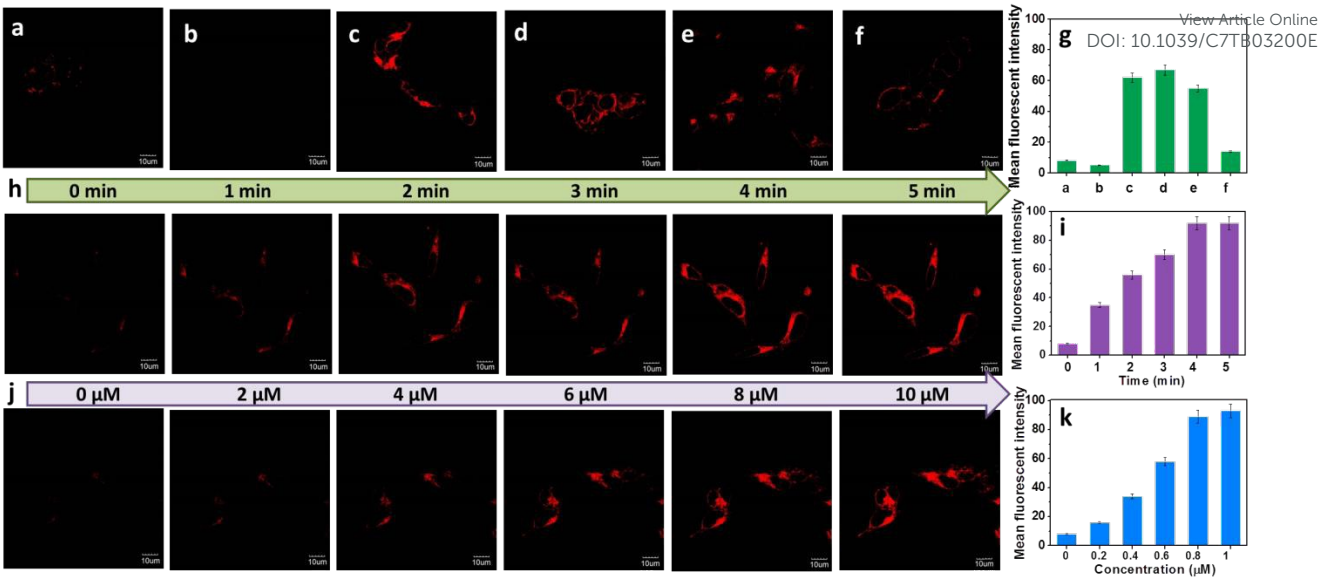

Fig. 2 Confocal microscopy images of SH-SY5Y cells for imaging sulfane sulfur using Mito-SH (1 μM). (a) Cells were pre-treated with Mito-SH for 20 min (a) and then incubated with Na_2S_4 (10 μM) for 20 min (c). (b) Cells were pretreated with NEM (5 mM) for 30 min before the same treatment with (a). (d) Cells were treated with 3H-1,2-dithiole-3-thione (10 μM) for 12 h and incubated with Mito-SH for 20 min. (e) Cells were treated with LPS (1 μg/mL) for 16 h, followed by incubated with Mito-SH for 20 min. (f) Cells were pretreated with PAG (1 mM) and then the same treatment with Fig. 2e. (g) Mean fluorescent intensity of flow cytometric analysis of (a)-(f). (h) Fluorescent images of SH-SY5Y cells with different incubation time. SH-SY5Y cells were pretreatment with Mito-SH and then loaded with various concentrations of Na_2S_4 (10 μM) with different incubated time (0-5 min). (i) Mean fluorescent intensity of flow cytometric analysis of (h). (j) Fluorescent images of SH-SY5Y cells with various concentrations. SH-SY5Y cells were pretreatment with Mito-SH and then loaded with various concentrations of Na_2S_4 (1-10 μM) for 20 min. (k) Mean fluorescent intensity of flow cytometric analysis of (j). Images were acquired using 635 nm excitation and emission intensities collected in optical windows between 700 and 800 nm. Scale bar: 10 μM.

Mitochondrial Sulfane Sulfur Detection in Living Cells

To further check the potential utilization of Mito-SH in bioimaging related fields, especially in cellular imaging, Mito-SH was applied for imaging sulfane sulfur in living cells. Initially, the viability of SH-SY5Y cells was examined in the presence of different concentrations of Mito-SH by a standard MTT assay (Fig. S3). The results revealed that more than 95% of cells still remained alive even at 20 μM Mito-SH. Moreover, no obvious cytotoxicity was observed even at a high concentration of Mito-SH (40 μM). The result suggested that our probe had low cytotoxicity and was suitable for imaging in living cells.

We next strived to detect sulfane sulfur in living cells using Mito-SH. SH-SY5Y cells in Figure 2a were incubated with 1 μM Mito-SH for 20 min, followed by washing of the cells with PBS buffer to remove the excessive probe. Cells in Figure 2b were pertreated with N-ethylmaleimide (NEM) for 30 min to deplete all the RSS, then the cells were incubated with 1 μM Mito-SH for 20 min. After treated the cells in Figure 2c as described in Figure 2a, Na_2S_4 (10 μM) was added into the Petri dish. Prior to imaging, all the cells were washed with PBS buffer for three times. The fluorescent images of SH-SY5Y cells were constructed using confocal laser scanning fluorescence microscopy with the excitation of a 635 nm laser. Cells in Figure 2a gave weaker fluorescence emission, indicating the low level of endogenous sulfane sulfur. There was no fluorescence signal in Figure 2b due to the addition of RSS scavenger NEM. In sharp contrast, a significantly increase in fluorescence intensity was visible upon addition of Na_2S_4 (Figure 2c). In addition, the increase of fluorescence intensities were concentration-dependent and time-dependent (Figure 2h and Figure 2j). The result demonstrated that the exogenous addition of Na_2S_4 could increase the intracellular concentration of sulfane sulfur. 3H-1,2-dithiole-3-thione now has been considered to be a therapeutic compounds as the source of sulfane sulfur in cells.[44] Thus, after treated with 3H-1,2-dithiole-3-thione (10 μM), a bright fluorescence signal was obtained in Figure 2d. These results confirmed that our probe Mito-SH could be successfully used to detect exogenous sulfane sulfur changes in living cells. Next, we investigated the application of Mito-SH for imaging of endogenous sulfane sulfur. The enzyme CSE has been reported to participate in sulfane sulfur generation.[7, 45, 46] the roles of the enzyme CSE in sulfane sulfur generation were following evaluated utilizing Mito-SH. CSE can overexpress via stimulating with lipopolysaccharide (LPS) in living cells.[47-49] The cells in Figure 2e were loaded with LPS (1 μg/mL) for 16 h, then incubated with Mito-SH for 20 min. As expected, an obvious fluorescence increase was observed. As a control group, the cells in Figure 2f were pretreated with a CSE inhibitor, DL-propargylglycine (PAG, 1 mM).[50] Subsequently, the cells in Figure 2f were undergone the same treatment as in Figure 2e. These cells provided much weaker fluorescence increase than Figure 2e. These results indicated that the probe was suitable for the detection of endogenous sulfane sulfur generated from enzyme CSE.

To evaluate the common applicability of Mito-SH, we further assessed the levels of sulfane sulfur in different cell lines, such as human lung carcinoma (A549) cells, mouse

Published on 05 February 2018. Downloaded by Fudan University on 06/02/2018 00:55:19.

Journal of Materials Chemistry B Accepted Manuscript

This journal is © The Royal Society of Chemistry 20xx

Please do not adjust margins

View Article Online
DOI: 10.1039/C7TB03200E

Published on 05 February 2018. Downloaded by Fudan University on 06/02/2018 00:55:19.

macrophage (RAW 264.7) cells, human hepatocellular liver carcinoma (HepG2) cells, human neuroblastoma (SH-SY5Y) cells, human cervical carcinoma (Hela) cells, human embryonic kidney (HEK) 293 cells, human hepatocellular liver carcinoma (HL-7702). The tested cell lines were pretreated with Mito-SH (1 μM) for 20 min as controls. Subsequently, the cell lines were loaded with Na_2S_4 (10 μM) for 20 min. As shown in Fig. 3, different weak fluorescent intensities were observed in controls, while the fluorescent intensities increased distinctly upon addition of Na_2S_4. Moreover, flow cytometry studies were constructed to confirm the results. These results demonstrated that the different cell lines preserved different endogenous levels of sulfane sulfur. And each cell lines provided different capabilities for exogenous sulfane sulfur. The results also displayed that our probe Mito-SH could be used to imaging sulfane sulfur in different cell lines.

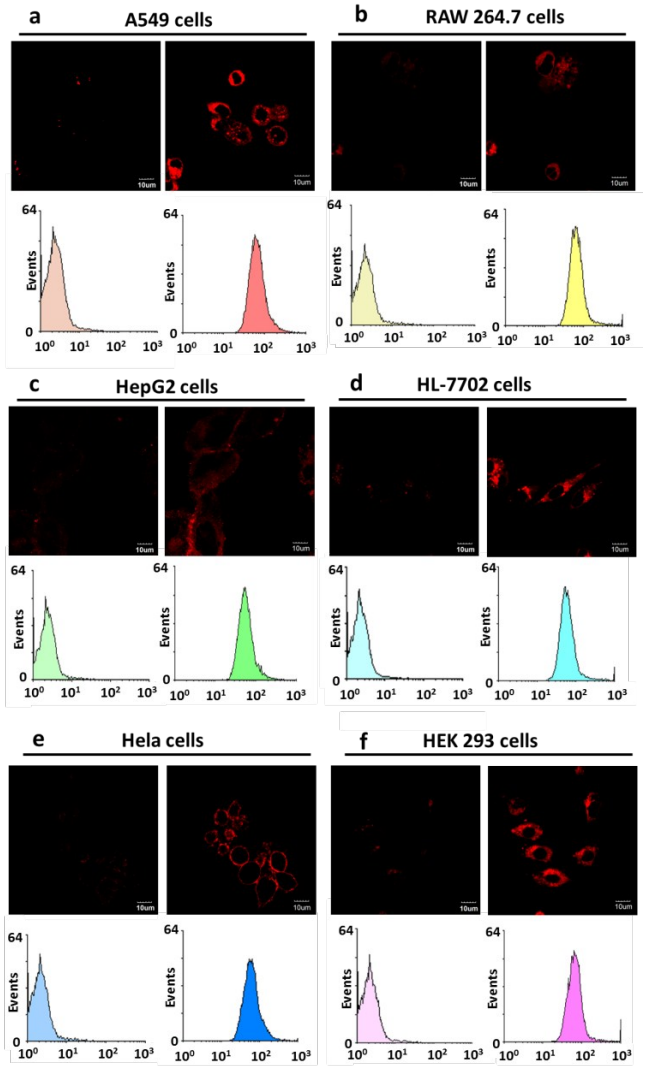

Fig. 3 Confocal microscopy images and flow cytometric analysis of different cell lines for imaging sulfane sulfur using Mito-SH (1 μM). (a) A549 cells; (b) RAW 264.7 cells; (c) HepG2 cells; (d) HL-7702 cells; (e) Hela cells; (f) HEK 293 cells. The cells in each group: the left cells were as controls, and the right cells were treated with Na_2S_4 (10 μM) for 20 min at 37 °C. All cell lines were preincubated with Mito-SH for 20 min and washed with PBS. Images were acquired using 635 nm excitation and emission intensities collected in optical windows between 700 and 800 nm. Scale bar: 10 μM.

Subcellular localization of Mito-SH

Mitochondria is the organelle in which produces energy. As the redox active center, mitochondria play a key role in maintaining cell health and apoptosis. Moreover, the mitochondrial respiratory chain is the prominent source of ROS during energy metabolism. Once stimulated, mitochondria produces too much ROS to be eliminated, and finally leading to oxidative stress. Long-time oxidative stress results in serious damage to cells and will induce many common diseases, such as cancer. About 60% of sulfane sulfur is held in mitochondria fraction, which efficiently protects cells from oxidative stress. In addition, sulfane sulfur also can be generated to directly confront oxidative stress. Therefore, a mitochondrial-targeting probe which can be used to detect mitochondrial sulfane sulfur is urgently required to further understand the physiological and pathological roles of sulfane sulfur. We predicted that our probe exhibited a significant ability to target mitochondria because of the lipophilic triphenylphosphonium cation. We next examined whether Mito-SH could detect the level changes of sulfane sulfur in mitochondria. The costaining dyes were a mitochondria tracker MitoTracker® Green FM and a DNA marker Hoechst 33342. Endogenous sulfane sulfur of SH- SH-SY5Y cells were overproduced via stimulated by LPS (1 μg/mL) for 16 h. Then a calcium ionophore A23187 (1 μM) was added to the above cells for 15 min to translate the enzyme CSE into mitochondria (Fig. 4a). After washed with PBS buffer, SH-SY5Y cells were stained with 1 μg/mL Hoechst 33342 for 30 min, 1 μg/mL MitoTracker® Green FM for 15 min, and 1 μM Mito-SH for 20 min. As shown in Fig. 4b, the probe could selectively respond to sulfane sulfur within 20 min. The fluorescent image of our probe was merged well with that of MitoTracker® Green FM (Fig. 4e). The Pearson's colocalization coefficient between Mito-SH and MitoTracker Green FM was calculated to be Rr = 0.91. The Manders' coefficients $m_1 = 0.89$, $m_2 = 0.94$. The results of the color–pair intensity correlation analysis displayed that only the pixel intensity distribution of Mito-SH and MitoTracker Green FM showed a high correlated plot (Fig. 4g). In addition, the intensity profiles of the linear regions of interest acrossed SH-SY5Y cells costained with Mito-SH and MitoTracker® Green FM (red arrow in Fig. 4e) were varying in close synchrony (Fig. 4j). The result illustrated that Mito-SH existed predominantly in the mitochondria. And our probe could selectively detect sulfane sulfur in the mitochondria.

Journal of Materials Chemistry B Accepted Manuscript

Please do not adjust margins

View Article Online
DOI: 10.1039/C7TB03200E

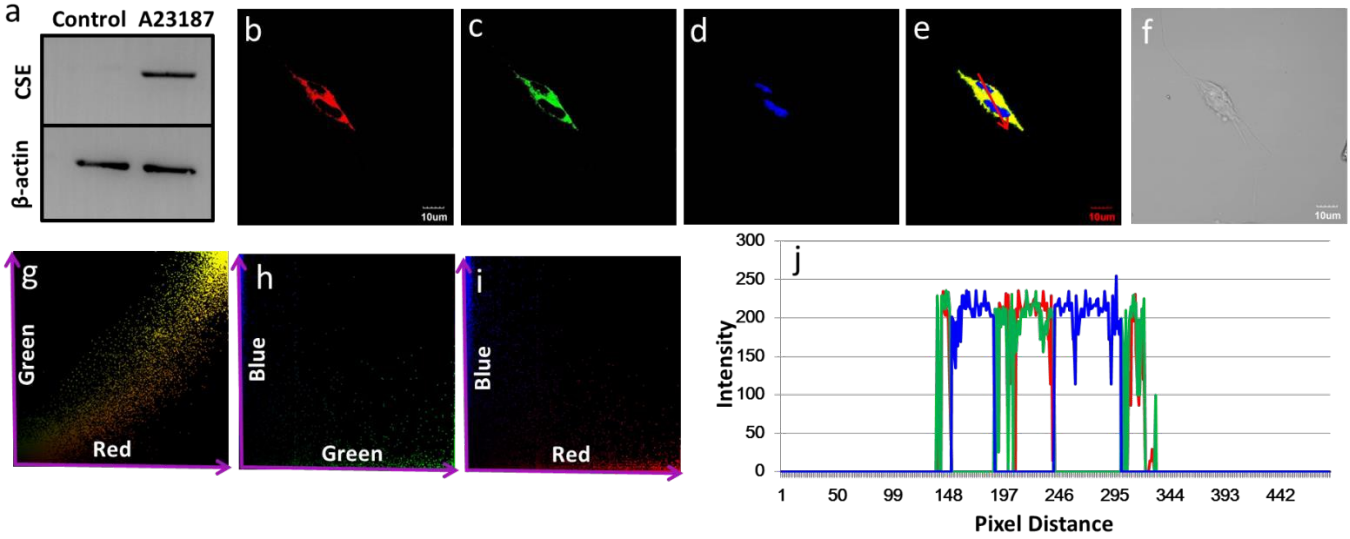

Fig. 4 (a) Western blot of CSE mitochondrial translocation induced by A23187 (1 μM). Confocal microscopy images of live SH-SY5Y cells costained by Mito-SH (1 μM, b), MitoTracker Green FM (1 μg/mL, c) and Hoechst 33342 (1 μg/mL, d). Images displayed represent fluorescence emission collected windows: 700–800 nm (λ_{ex} = 635 nm) for Mito-SH; 500–580 nm (λ_{ex} = 488 nm) for MitoTracker® Green FM; 425-500 nm (λ_{ex} = 405 nm) for Hoechst 33342. (e) Overlay image of (b) and (c). (f) Bright-field of (b). (g) Displayed the colocalization areas of the red and green channels. (h) Displayed the colocalization areas of the blue and green channels selected. (i) Displayed the colocalization areas of the red and blue channels selected. (j) Intensity profile of regions of interest (red arrow in panel e) across SH-SY5Y cells.

Imaging of sulfane sulfur changes in oxygen-glucose deprived models

Ischemia is caused by the deficiency of blood supply to a limited area of tissue. The insufficiency of blood supply will affect the expression of many proteins, which may cause destruction in the ischemic tissue. Many evidences indicate that the ischemia-induced injury can originate from the excessive production of ROS. [51-53] Oxidative damage to DNA and other biological macromolecules result in cell necrotic or apoptotic.[54] As an important family of the cellular antioxidant defense systems, sulfane sulfur protects cells against the damage caused by oxidative stress and maintains the cellular redox homeostasis.[55] Therefore, we wanted to investigate the dynamic level changes of sulfane sulfur during ischemia. Oxygen-glucose deprivation (OGD) can mimic the acute restriction of metabolite and oxygen supply caused by ischemia. Thus, Mito-SH was applied to detect the change of sulfane sulfur in living cells under OGD. We utilized SH-SY5Y cells, A549 cells, HEK 293 cells, and HL-7702 cells to exploit this test. As illustrated in Figure 5a, each cell lines were divided into five groups. Briefly, all cell lines in group a were loaded with Mito-SH and cultured with Dulbecco's Modified Eagle Medium (DMEM)/ Roswell Park Memorial Institute 1640 (RPMI 1640)/ Minimum Essential Medium (MEM) containing 25 mM glucose as control under normal condition. The cells in group b were incubated with Mito-SH and cultured with glucose-free DMEM/RPMI 1640/MEM under 0.1% oxygen level. 2-deoxyglucose (2DG) is a relatively nontoxic analog of glucose, which has been investigated as potential glucose antimetabolites to inhibit glycolysis. The competition uptake between 2DG and glucose will lead to the inhibition of glucose metabolism, which also can result in glucose deprivation.[56] The cells in group c were pretreated with 2DG for 3 hours and then incubated with Mito-SH for another 20 min under 0.1% oxygen level. As expected, the cells of Group b and Group c offered clear fluorescence signals emission. The results indicated that sulfane sulfur had been generated after the stimulation of OGD. The control cells exhibited much weaker fluorescence. These results demonstrated that our probe could be used to image sulfane sulfur in living cells under OGD. Moreover, cellular apoptosis induced by OGD was further assessed using PE Annexin V/7-AAD assay. As shown in Fig. 5b, flow cytometry analysis indicated that the cells in group b and group c displayed apoptosis rate (including necrosis) as 9.5% and 8.9%, 18.1% and 19.8%, 37.8% and 28.3%, 33.9% and 32.8% in SH-SY5Y cell line, A549 cell line, HEK 293 cell line, HL-7702 cell line, respectively. However, the apoptosis rate of group a was 4.4%, 6.5%, 8.5% and 9.8% in SH-SY5Y cell line, A549 cell line, HEK 293 cell line, HL-7702 cell line, respectively. All cell lines underwent apoptosis after OGD. However, cancer cells exhibited relatively low apoptosis rate than normal cells, indicating that cancer cells were more tolerant than normal cells toward OGD. To test whether OGD resulted in caspase-dependent apoptosis, we selected SH-SY5Y cell line to assess the caspase activities using a colorimetric peptide substrate for caspase Ac-DEVD-pNA. As shown in Fig. 5c, the absorbance increased in group b and c under OGD. In addition, no caspase activities were observed after addition of caspase inhibitor Ac-DEVD-CHO. Thus, OGD could activate caspase activities in group b and group c. Release of cytochrome *c* from mitochondria into cytosol is an important step during caspase-dependent apoptosis. Cytochrome c once binds to Apaf-1 in cytosol, it will trigger the activation of caspase-9. Subsequently, caspase-3 is activated through the cleavage of procaspase-3.[57] In this test, we found that cytochrome *c* was

Published on 05 February 2018. Downloaded by Fudan University on 06/02/2018 00:55:19.

Journal of Materials Chemistry B Accepted Manuscript

This journal is © The Royal Society of Chemistry 20xx

Please do not adjust margins

released into cytosol and cleaved-caspase-3 was generation after the simulation of OGD. We also evaluated the cleavage of a cellular substrate of caspase poly(ADP-ribose) polymerase (PARP) using western blotting assay. The cleaved product of PARP was detected in these OGD-simulating cells. Next, we tried to investigate whether sulfane sulfur could act cytoprotective roles against ischemia or not. Before treated by OGD which had described as group b and group c, the cells in group d and group e were pretreated with Na_2S_4 (100 μM) for 20 min. Compared with the cells without addition of Na_2S_4, co-incubation with Na_2S_4 significantly increased the fluorescence of Mito-SH. Importantly, the cells with the addition of Na_2S_4 offered an obviously lower apoptosis rate (Fig. 5b). These cells did not release a great deal of cytochrome *c* from mitochondria into cytoplasm. The cleaved product of caspase-3 was lowly expressed (Fig. 5d and Fig. 5e). Only few cleaved product of PARP was found in these cells. These results may attribute to the cytoprotective roles of sulfane sulfur.

View Article Online DOI: 10.1039/C7TB03200E

Published on 05 February 2018. Downloaded by Fudan University on 06/02/2018 00:55:19.

Journal of Materials Chemistry B Accepted Manuscript

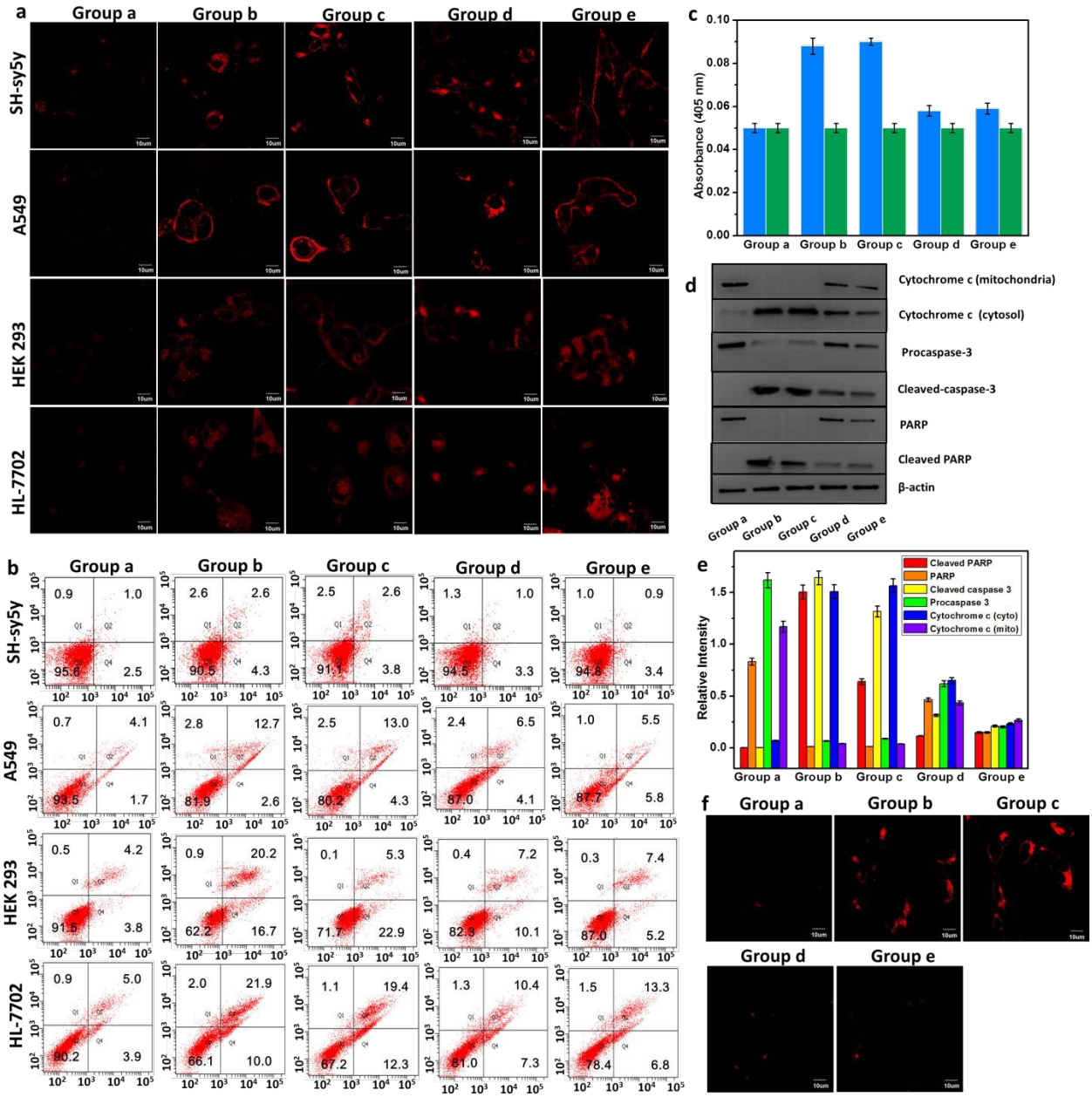

Fig. 5 (a) Confocal fluorescence images of Mito-SH for detection of sulfane sulfur in different cell lines under OGD. All the cells were loaded with Mito-SH (1 μM) for 15 min. Group a were cultured with DMEM/RPMI 1640/MEM containing 25 mM glucose for 3 h. Group b were cultured with glucose-free DMEM under 0.1% O_2 for 3 h. Group c were pre-treated with 2DG for 3 h and then cultured under 0.1% O_2. The cells were pretreated with Na_2S_4 (100 μM) for 20 min and then the same treatment with Group c (Group d) and Group d (Group e). (b) Annexin V and 7-AAD assays of living cells in Group a, b, c, d and e using flow cytometry analysis. Untreated cells are used as a control. Q1: necrosis cells, Q2: late apoptotic cells, Q3: survival cells, Q4: early apoptotic cells. Numbers inserted in the graphs represent the percentages of each part in the whole cells. (c) Caspase activities of lysates of SH-SY5Y cells in Group a, b, c, d and e were measured by using 200 μM Ac-DEVD-pNA in the absence and presence of 20 μM Ac-DEVD-CHO (mean ± s.d., n=3). (d) Western Blotting of SH-SY5Y cells in Group a, b, c, d and e were conducted using the corresponding antibodies. β-Actin was used as a loading control. (e) The relative intensity analysis of proteins in Fig. (d) by Image pro-plus software. (f) Confocal fluorescence images of Hydro-IR-783 (1 μM) in SH-SY5Y cells for the detection of ROS.

Please do not adjust margins

View Article Online
DOI: 10.1039/C7TB03200E

Published on 05 February 2018. Downloaded by Fudan University on 06/02/2018 00:55:19.

To confirm cytoprotective effects of sulfane sulfur against oxidative damage through scavenging ROS, ROS level was then assessed using a ROS probe Hydro-IR-783 in SH-SY5Y cells. The results were displayed in Fig. 5f, the generation of ROS was upregulated during the stimulation of OGD. While after addition of Na_2S_4, the fluorescence signal of Hydro-IR-783 decreased. The results demonstrated that the level of ROS was burst produced during OGD process. Sulfane sulfur could directly eliminate ROS in cells. It is easy to conclude that sulfane sulfur had exhibited cytoprotective roles via scavenging ROS. That was, after OGD stress, the living cells attempt to upregulate sulfane sulfur for compensating OGD-induced oxidative stress.

Imaging sulfane sulfur in acute brain ischemia

Fluorescent probe functions in the NIR region (650 - 900 nm) can penetrate deep tissues and reduce the interference of background autofluorescence. Therefore, our probe is a preferential candidate for fluorescent imaging of sulfane sulfur in vivo (Fig. S5). A continuous supply of nutrients, especially glucose and oxygen from the blood, are essential for brain to satisfy the energy demands. The brain is susceptible to oxygen because it bears 2% -3% of the body's weight while it requires 20% of the body's oxygen. Ischemia of brain will induce the overproduction of ROS.[58] These ROS will irreversibly destroy the functions of cells, which eventually resulted in brain damage and neurological dysfunction. We now attempted to image the level changes of sulfane sulfur during brain ischemia. Meanwhile, we also evaluated whether sulfane sulfur possessed the protective ability during brain ischemia. As illustrated in Fig. 6, the BALB/c mice were divided into two groups. One is the ischemia group I, and the other is the therapy group II. Bilateral carotid arteries of mice in ischemia group were ligated for 0, 5, 10, 15, 20, 25, 30 min to build brain ischemia model of mice. While the mice in therapy group were with intravenous injection of sulfane sulfur (Na_2S_4, 10 μM) and maintained with 1 h before the same treatment with the ischemia group. Then the brain was immediately isolated and hippocampus tissues were dissected using a vibration slicer under anaerobic environment. The levels of sulfane sulfur were detected in hippocampus tissues using Mito-SH. As shown in Fig. 6b, moderate fluorescence signal was observed in the mice without ligation at 0 min. The moderate fluorescence signal was attributed to the endogenous sulfane sulfur. Once ligation occurred, the hippocampus immediately emitted obvious fluorescence even within 5 min. The fluorescent intensity was positively correlation with the ligation time and statured in 15 min, followed by a decrease in fluorescence intensity. For the therapy group II, the fluorescence signals underwent the same trend which was similar with the ischemia group I. However, the overall fluorescence intensities in group II were higher than group I, indicating that the supplement of exogenous sulfane sulfur would increase the intracellular level of sulfane sulfur. We further surveyed the changes of ROS in the hippocampus using Hydro-IR-783. As illustrated in Fig. 6c, there existed a level increase of ROS which occurred at the ligation of bilateral carotid arteries. It was reasoned that the suddenly increase of sulfane sulfur should be used to remove the excessive generation of ROS (Fig. 6b). However, sulfane sulfur could not get an effective supplement with the extension time of ligation. Therefore, we obtain a weak fluorescent image at 30 min, which showed the detection of ROS. In the therapy group II, the ROS level was always constrained by the addition of exogenous sulfane sulfur (Fig. 6i). The normalized fluorescent intensities were displayed in Fig. S6.

Reperfusion can aggravate the functional metabolic disorders and structural damage of body. Thus, the phenomenon of increased injury after the recovery of blood supply has been known as ischemia-reperfusion injury. We hypothesized that the levels of sulfane sulfur and ROS must experience a series of intricate changes during the process of ischemia-reperfusion. Therefore, grasping real-time information of between sulfane sulfur and ROS would facilitate understanding their biological roles. We next detected the level changes of sulfane sulfur and ROS during ischemia-reperfusion process at different time points. As shown in Fig. 6b, the fluorescent intensity of Mito-SH in group I was sharply decreased at 5 min reperfusion. And the fluorescent image was maintained at low fluorescence level, indicating the low level of sulfane sulfur. While the fluorescent intensity of Hydro-IR-783 in group I exhibited dramatic rise at the 5 min reperfusion and there was a slight decrease from 30 min to 120 min, suggesting the burst of ROS generation during the early stage of reperfusion (Fig. 6c). Compared with group I, the hippocampus of mice in group II showed low fluorescent intensity of Mito-SH, but there was a slight fluorescence increase at the late stage of reperfusion (Fig. 6h). Meanwhile, the probe Hydro-IR-783 displayed weak fluorescent intensity, illustrating the low level of ROS (Fig. 6i).

Journal of Materials Chemistry B Accepted Manuscript

This journal is © The Royal Society of Chemistry 20xx

Please do not adjust margins

View Article Online
DOI: 10.1039/C7TB03200E

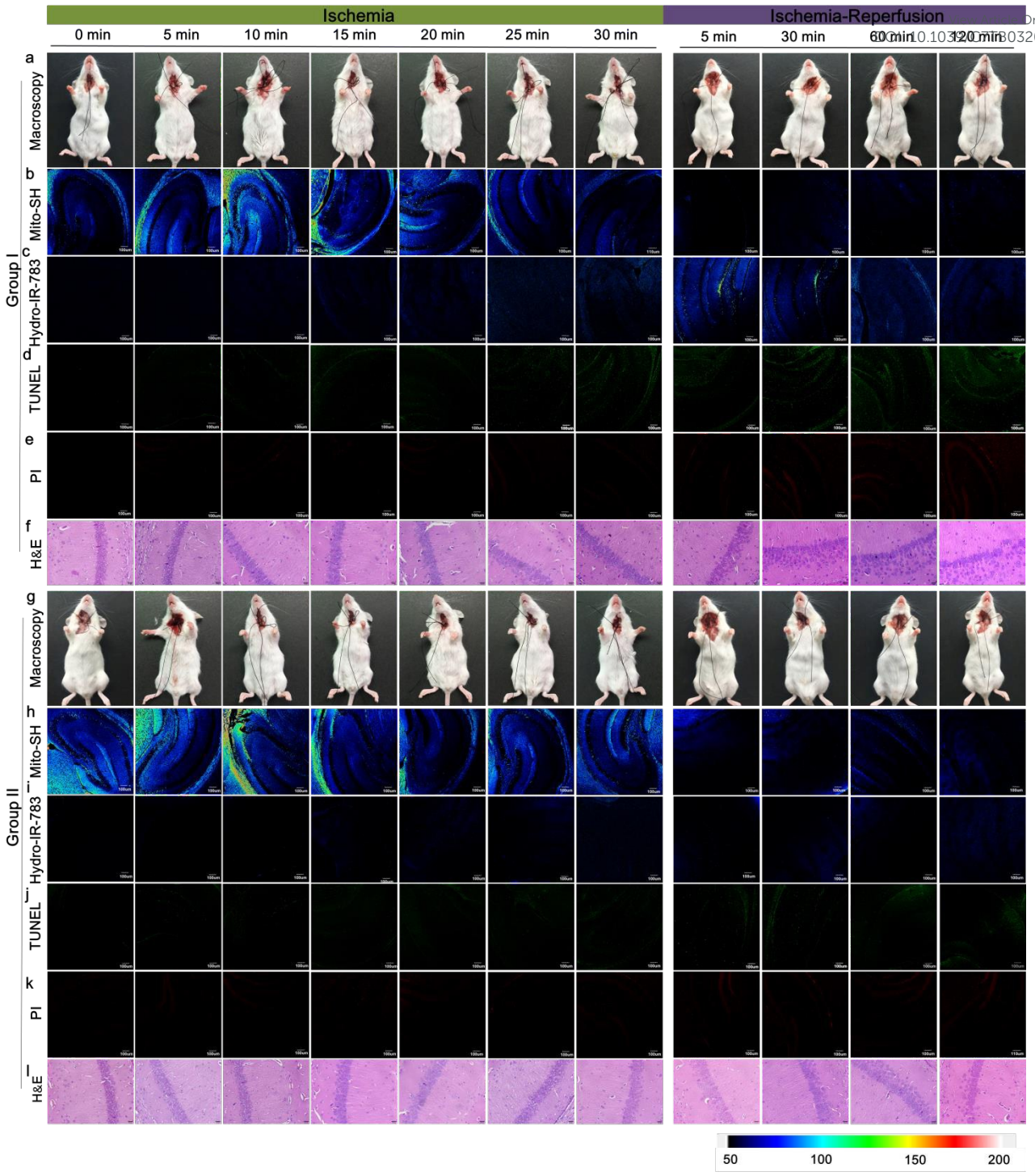

Fig. 6. The analysis of hippocampal slices in mice model of ischemia-reperfusion. Group I: the mice were ligated bilateral carotid arteries for 0, 5, 10, 15, 20, 25, 30 min and then reprimed for 0, 30, 60, 120 min. Group II: the mice were intravenous injection of Na_2S_4 (10 μM) and maintained with 1 h before the same treatment with group I. (a) and (g) Macropathology images of mice model of brain ischemia. (b) and (h) Representative fluorescent images of hippocampal slice stained with Mito-SH (1 μM) for 20 min. Scale bar: 100 μm. (c) and (i) Representative fluorescent images of hippocampal slice stained with Hydro-IR-783 (1 μM) for 20 min. Scale bar: 100 μm. (d) and (j) TUNEL assay of hippocampal slices in different mices. (e) and (k) PI assay of hippocampal slices in different mices. Scale bar: 100 μm. (f) and (l) Representative slides of H&E-stained hippocampal from group I and group II. Scale bar: 20 μm.

To evaluate the apoptosis cells induced by ischemia-reperfusion, TUNEL staining was used in hippocampus slices of group I and group II. As shown in Fig. 6d, the hippocampus of control mice in group I did not exhibit dramatic fluorescence. All the other hippocampus slices exhibited increasing green fluorescence after ischemia 5 min, 10 min, 15 min, 20 min, 25 min, and 30 min. And stronger fluorescent intensities occurred during reperfusion. Obviously, the fluorescent intensities in group II were much lower than those in group I (Fig. 6j), suggesting the relative less cell apoptosis in group II. These

Published on 05 February 2018. Downloaded by Fudan University on 06/02/2018 00:55:19.

Journal of Materials Chemistry B Accepted Manuscript

Please do not adjust margins

View Article Online
DOI: 10.1039/C7TB03200E

Published on 05 February 2018. Downloaded by Fudan University on 06/02/2018 00:55:19.

Journal of Materials Chemistry B Accepted Manuscript

results demonstrated that sulfane sulfur could exhibit protective role in ischemia-reperfusion injury. That was, the appropriate amount of exogenous sulfane sulfur could reduce oxidative damage during the process of ischemia-reperfusion. We also assessed the cell necrosis induced by ischemia-reperfusion using PI staining. As shown in Fig. 6e and Fig. 6k, the red fluorescent intensities of hippocampus showed a continuous rise both in group I and group II. As expected, the fluorescent intensities in group I were lower than those in group II. These results further confirmed the protective effects of sulfane sulfur against oxidative stress. In addition, ischemia induce injury was assessed by H&E (hematoxylin and eosin) staining. The CA1 region of hippocampus was collected for analysis. After ischemia, the cells in group I loosely arranged (Fig. 6f). And the nucleus appeared shapedness. Cell morphology showed more severe during the ischemia-reperfusion process. However, as illustrated in group II, the administration of exogenous sulfane sulfur could effectively improve this situation.

Conclusions

In this work, we develop a mitochondrial-specific fluorescent probe Mito-SH for the evaluation of sulfane sulfur in oxygen-glucose deprived cell models and in acute ischemia mice models. The lipophilic triphenylphosphonium cation can guide the probe into mitochondria. The mercapto (-SH) response unit can selectively respond to the reactive sulfur atom thiosulfoxide (the tautomerization of sulfane sulfur) to trigger remarkable NIR fluorescence emission changes of *azo*-BODIPY fluorophore. The probe exhibits high selectivity, good photostability and low cytotoxicity when used in the tests. Owing to these excellent properties, Mito-SH has been applied for imaging of sulfane sulfur dynamic changes in cells under oxygen-glucose deprivation. Sulfane sulfur can behave cytoprotective roles against oxidative damage caused by oxygen-glucose deprivation. Moreover, Mito-SH has been successfully utilized to imaging sulfane sulfur in acute ischemia mice models. Acute ischemia can lead to a burst produce of ROS in the hippocampus, and sulfane sulfur functions physiological protection via directly eliminating ROS. However, severe oxidative damage of the hippocampus is irreversible, it will promote cell apoptosis and necrosis. All these results feature that our probe Mito-SH can serve as a potential tool for exploring functions of sulfane sulfur in cells and in vivo.

Experimental

Synthesis of Mito-SH

The synthesis of Mito-SH was shown in Scheme S1. Mito-1 was synthesized from our lab.[27] Mito-1 (92.6 mg, 0.1 mmol), 1-ethyl-3-(3-dimethylaminopropyl) carbodiimide hydrochloride (EDC, 38.4 mg, 0.2 mmol), 4-dimethylaminopyridine (DMAP, 2.44 mg, 0.02 mmol), and 2,2'-disulfanediyldibenzoic acid (61.2 mg, 0.2 mmol) were added into 50 mL anhydrous CH_2Cl_2 under Ar condition. The reaction was lasted for 12 hours at 25 °C. Then the mixture was neutralized with dilute HBr and extracted with CH_2Cl_2 (50 mL × 3). The organic layer were evaporated and the resulting residue was subjected to column chromatography for purification (eluent CH_2Cl_2). Then the afforded product was further reacted with DL-Dithiothreitol (DTT, 15.4 mg, 0.1 mmol) for 2 h in ethanol (30 mL) under Ar atmosphere at room temperature. The organic layer was extracted with CH_2Cl_2 (50 mL × 3), dried over sodium sulfate and evaporated under reduced pressure. The crude product of Mito-SH was purified by column chromatography (eluent CH_2Cl_2). The final product was obtained as dark green crystals, 31.8 mg, and yield 30%. ^{1}H NMR (500 MHz, $CDCl_3$-D_1) δ(ppm): 8.06-7.85 (m, 10H), 7.63-7.52 (m, 12H), 7.35-7.32 (m, 7H), 7.25-7.23 (q, 2H), 7.15-7.09 (m, 3H), 7.00-6.96 (m, 4H), 6.66-6.64 (d, 1H, *J* = 10 Hz), 5.50 (s, 1H), 3.99-3.92 (t, 2H, *J* = 17.5 Hz), 3.69-3.62 (t, 2H, *J* = 17.5 Hz), 2.95-2.87 (m, 2H), 1.92-1.80 (m, 2H). ^{13}C NMR (125 MHz, $CDCl_3$-D_1) δ (ppm): 167.86, 162.00, 157.21, 154.06, 153.51, 151.59, 146.92, 134.99, 133.50, 133.42, 132.91, 132.48, 131.96, 130.93, 130.51, 128.52, 130.41, 130.04, 129.75, 129.30, 129.16, 128.52, 127.26, 125.96, 123.52, 118.48, 117.16, 114.67, 101.47, 69.39, 31.94, 29.71, 27.35, 22.70. LC-MS (ESI+): m/z $C_{61}H_{48}BF_2N_3O_3PS^+$ calcd. 982.3210, found [M^+] 982.3211. Elemental Analysis: calcd. C, 68.94; H, 4.55; N, 3.95; P, 2.91; S, 3.02. Found C, 68.96; H, 4.56; N, 3.93; P, 2.90; S, 3.01.

Cell culture and confocal imaging

A549 cells, RAW 264.7 cells, HL-7702 cells, SH-SY5Y cells were cultured in RPMI 1640 medium supplemented with 10% fetal bovine serum (FBS) at 37 °C in an atmosphere of 5 % CO_2 and 95 % air. Hela cells and HepG2 cells were cultured in DMEM medium supplemented with 10% FBS at 37 °C in an atmosphere of 5 % CO_2 and 95 % air. HEK 293 cells were cultured in MEM medium supplemented with 10% FBS at 37 °C in a humidified atmosphere containing 5% CO_2. Prior to imaging, the cells were washed with PBS for three times. Fluorescent images were acquired on an Olympus Fluo View FV1000 confocal laser-scanning microscope (Japan) with an objective lens (×60). The excitation wavelength was 635 nm. 0.1% O_2 concentration was generated with an AnaeroPack™.

Photostability in cells

The cells were cultured with Na_2S_4 (1.0 μM) for 15 min and then loaded with 1.0 μM Mito-SH for 20 min at 37 °C in an atmosphere of 5 % CO_2 and 95 % air, and then the fluorescent intensity was constructed. The changes of fluorescent intensity with scan time were determined by confocal laser scanning microscope (Japan Olympus Co., Ltd) for 480 min. The intensity of Mito-SH was recorded with the emission in the range of 700-800 nm and the excitation wavelength at 635 nm. The data were obtained from replicate experiments (n=5).

Oxygen-glucose deprivation condition in cell incubation

For the real-time live-cell imaging of oxygen-glucose deprivation, the cells were incubated with Mito-SH and cultured with glucose-free RPMI 1640/DMEM/MEM medium supplemented with 10% FBS at 37 °C under 0.1% O_2. The cells

This journal is © The Royal Society of Chemistry 20xx

Please do not adjust margins

were loaded with Mito-SH and cultured with RPMI 1640/DMEM/MEM medium containing 25 mM glucose at 37 °C in a 5% CO_2 incubator as control.

Preparation of acute ischemia mice modals and hippocampal slices

BALB/c mice, 20-25 g, were purchased from Binzhou Medical University. Mice were group-housed on a 12:12 light–dark cycle at 22 °C with free access to food and water. In-vivo images was achieved by IVIS Lumina XRMS Series Ⅲ (Perkinelmer, USA). All surgical procedures were conducted in conformity with National Guidelines for the Care and Use of National Guidelines for the Care and Use of Laboratory Animals Laboratory Animals, and experimental protocols were approved by the Institutional Animal Care and Use Committee in Binzhou Medical University, Yantai, China. Approval Number: No. BZ2014-102R. For acute ischemia mice, bilateral carotid arteries of mice were ligated for 0, 5, 10, 15, 20, 25 and 30 min to build acute ischemia mice models. The lines pass through the vessel without ligation in mice were set as control. Subsequently, the hippocampal slices were prepared by vibration slicer at oxygen-free operator station and incubated with 10 μM Mito-SH for 20 min.

Conflicts of interest

There are no conflicts to declare.

Acknowledgements

We thank the National Nature Science Foundation of China (No. 21575159, No. 21775162, No. 41776110, and No. 21405172), the program of Youth Innovation Promotion Association, CAS (Grant 2015170), State Key Laboratory of Environmental Chemistry and Ecotoxicology, Research Center for Eco-Environmental Sciences, CAS (Grant KF2016-22), the Instrument Developing Project of the CAS (YZ201662), and Key Laboratory of Sensor Analysis of Tumor Marker Ministry of Education, Qingdao University of Science and Technology (Grant SATM201705).

Notes and references

1 R. D. Guzy, B. Hoyos, E. Robin, H. Chen, L. Liu, K. D. Mansfield, M. C. Simon, U. Hammerling and P. T. Schumacker, *Cell Metab.*, 2005, **1**, 401-408.
2 P. K. Yadav, M. Martinov, V. Vitvitsky, J. Seravalli, R. Wedmann, M. R. Filipovic and R. Banerjee, *J. Am. Chem. Soc.*, 2016, **138**, 289-299.
3 J. I. Toohey and A. J. Cooper, *Molecules*, 2014, **19**, 12789-12813.
4 M. H. Stipanuk and P. W. Beck, *Biochem. J.*, 1982, **206**, 267-277.
5 J. I. Toohey, *Anal. Biochem.*, 2011, **413**, 1-7.
6 X. Shen, E. A. Peter, S. Bir, R. Wang and C. G. Kevil, *Free Radical Bio. Med.*, 2012, **52**, 2276-2283.
7 T. Ida, T. Sawa, H. Ihara, Y. Tsuchiya, Y. Watanabe, Y. Kumagai, M. Suematsu, H. Motohashi, S. Fujii, T. Matsunaga, M. Yamamoto, K. Ono, N. O. Devarie-Baez, M. Xian, J. M. Fukuto and T. Akaike, *P. Natl. Acad. Sci. USA*, 2014, **111**, 7606-7611.
8 Y. Kimura, Y. Mikami, K. Osumi, M. Tsugane, J. i. Oka and H. Kimura, *Faseb. J*, 2013, **27**, 2451-2457.
9 H. Kimura, *Antioxida. redox sign.*, 2015, **22**, 347-349.
10 H. Kimura, *Molecules*, 2014, **19**, 16146-16157.
11 T. Ida, T. Sawa, H. Ihara, Y. Tsuchiya, Y. Watanabe, Y. Kumagai, M. Suematsu, H. Motohashi, S. Fujii and T. Matsunaga, *P. Natl. Acad. Sci. USA*, 2014, **111**, 7606-7611.
12 K. Ono, T. Akaike, T. Sawa, Y. Kumagai, D. A. Wink, D. J. Tantillo, A. J. Hobbs, P. Nagy, M. Xian and J. Lin, *Free Radical Bio. Med.*, 2014, **77**, 82-94.
13 R. Munday, J. S. Munday and C. M. Munday, *Free Radical Bio. Med.*, 2003, **34**, 1200-1211.
14 D. Xiao, A. Herman-Antosiewicz, J. Antosiewicz, H. Xiao, M. Brisson, J. S. Lazo and S. V. Singh, *Oncogene*, 2005, **24**, 6256-6268.
15 J. L. Wood, *Method. Enzymol.*, 1987, **143**, 25-29.
16 Y. Takano, K. Shimamoto and K. Hanaoka, *J. Clin. Biochem. Nutr*, 2016, **58**, 7-15.
17 F. Yu, X. Han and L. Chen, *Chem. Commun.*, 2014, **50**, 12234-12249.
18 V. S. Lin, W. Chen, M. Xian and C. J. Chang, *Chem. Soc. Rev.*, 2015, **44**, 4596-4618.
19 X. Chen, Y. Zhou, X. Peng and J. Yoon, *Chem. Soc. Rev.*, 2010, **39**, 2120-2135.
20 Y. Yang, Q. Zhao, W. Feng and F. Li, *Chem. Rev.*, 2012, **113**, 192-270.
21 H. S. Jung, X. Chen, J. S. Kim and J. Yoon, *Chem. Soc. Rev.*, 2013, **42**, 6019-6031.
22 M. Gao, F. Yu, C. Lv, J. Choo and L. Chen, *Chem. Soc. Rev.*, 2017, **46**, 2237-2271.
23 N. Jiang, J. Fan, F. Xu, X. Peng, H. Mu, J. Wang and X. Xiong, *Angew. Chem. Int. Edit.*, 2015, **54**, 2510-2514.
24 J. Fan, M. Hu, P. Zhan and X. Peng, *Chem. Soc. Rev.*, 2013, **42**, 29-43.
25 W. Chen, C. Liu, B. Peng, Y. Zhao, A. Pacheco and M. Xian, *Chem. Sci.*, 2013, **4**, 2892-2896.
26 Y. Takano, K. Hanaoka, K. Shimamoto, R. Miyamoto, T. Komatsu, T. Ueno, T. Terai, H. Kimura, T. Nagano and Y. Urano, *Chem. Commun.*, 2017, **53**, 1064-1067.
27 M. Gao, F. Yu, H. Chen and L. Chen, *Anal. Chem.*, 2015, **87**, 3631-3638.
28 L. Zeng, S. Chen, T. Xia, W. Hu, C. Li and Z. Liu, *Anal. Chem.*, 2015, **87**, 3004-3010.
29 Q. Han, Z. Mou, H. Wang, X. Tang, Z. Dong, L. Wang, X. Dong and W. Liu, *Anal. Chem.*, 2016, **88**, 7206-7212.
30 H. Shang, H. Chen, Y. Tang, R. Guo and W. Lin, *Sensor. Actuat. B-chem*, 2016, **230**, 773-778.
31 W. Chen, E. W. Rosser, D. Zhang, W. Shi, Y. Li, W.-J. Dong, H. Ma, D. Hu and M. Xian, *Org. Lett.*, 2015, **17**, 2776-2779.
32 W. Chen, E. W. Rosser, T. Matsunaga, A. Pacheco, T. Akaike and M. Xian, *Angew. Chem. Int. Edit.*, 2015, **54**, 13961-13965.
33 W. Chen, A. Pacheco, Y. Takano, J. J. Day, K. Hanaoka and M. Xian, *Angew. Chem. Int. Edit.*, 2016, **55**, 9993-9996.
34 C. Liu, W. Chen, W. Shi, B. Peng, Y. Zhao, H. Ma and M. Xian, *J. Am. Chem. Soc.*, 2014, **136**, 7257-7260.
35 N. Gupta, S. I. Reja, V. Bhalla and M. Kumar, *Org. Biomol. Chem.*, 2017, **15**, 6692-6701.
36 F. Yu, M. Gao, M. Li and L. Chen, *Biomaterials.*, 2015, **63**, 93-101.
37 Y. Huang, F. Yu, J. Wang and L. Chen, *Anal. Chem.*, 2016, **88**, 4122-4129.
38 X. Han, F. Yu, X. Song and L. Chen, *Chem. Sci.*, 2016, **7**, 5098-5107.
39 X. Song, H. Bian, C. Wang, M. Hu, N. Li and Y. Xiao, *Org.*

View Article Online DOI: 10.1039/C7TB03200E

Published on 05 February 2018. Downloaded by Fudan University on 06/02/2018 00:55:19.

Journal of Materials Chemistry B Accepted Manuscript

Please do not adjust margins

View Article Online
DOI: 10.1039/C7TB03200E

Biomol. Chem., 2017, **15**, 8091-8101.
40 X. Song, M. Hu, C. Wang and Y. Xiao, *RSC Adv.*, 2016, **6**, 69641-69646.
41 J. Zhang, M. Yang, C. Li, N. Dorh, F. Xie, F.-T. Luo, A. Tiwari and H. Liu, *J. Mater. Chem. B*, 2015, **3**, 2173-2184.
42 K. Dou, G. Chen, F. Yu, Z. Sun, G. Li, X. Zhao, L. Chen and J. You, *J. Mater. Chem. B*, 2017, **5**, 8389-8398.
43 L. Yuan, W. Lin, K. Zheng, L. He and W. Huang, *Chem. Soc. Rev.*, 2013, **42**, 622-661.
44 J. I. Toohey and A. J. L. Cooper, *Molecules*, 2014, **19**, 12789-12813.
45 N. Shibuya, M. Tanaka, M. Yoshida, Y. Ogasawara, T. Togawa, K. Ishii and H. Kimura, *Antioxid. redox sign.*, 2009, **11**, 703-714.
46 J. Ma, J. Fan, H. Li, Q. Yao, F. Xu, J. Wang and X. Peng, *J. Mater. Chem. B*, 2017, **5**, 2574-2579.
47 X. Zhu, S. Liu, Y. Liu, S. Wang and X. Ni, *Cell. Mol. Life Sci.*, 2010, **67**, 1119-1132.
48 H. Jurkowska, W. Placha, N. Nagahara and M. Wrobel, *Amino Acids*, 2011, **41**, 151-158.
49 H. Jurkowska and M. Wrobel, *Amino Acids*, 2008, **34**, 231-237.
50 D. W. Porter and S. I. Baskin, *J. biochem. Toxic.*, 1996, **11**, 45-50.
51 S. Love, *Brain Pathol.*, 1999, **9**, 119-131.
52 K. Niizuma, H. Endo and P. H. Chan, *J. Neurochem.*, 2009, **109**, 133-138.
53 J. M. McCord, *New Engl. J. Med.*, 1985, **312**, 159-163.
54 E. Noiri, A. Nakao, K. Uchida, H. Tsukahara, M. Ohno, T. Fujita, S. Brodsky and M. S. Goligorsky, *Am. J. Physiol – Renal.*, 2001, **281**, F948-F957.
55 J. I. Toohey, *Biochem. J.*, 1989, **264**, 625.
56 A. L. Simons, D. M. Mattson, K. Dornfeld and D. R. Spitz, *J. Cancer Res. Ther.*, 2009, **5**, 2-6.
57 P. Li, D. Nijhawan, I. Budihardjo, S. M. Srinivasula, M. Ahmad, E. S. Alnemri and X. D. Wang, *Cell*, 1997, **91**, 479-489.
58 L. B. Becker, T. L. vanden Hoek, Z. Shao, C. Li and P. T. Schumacker, *Am. J. Physiol – Heart.*, 1999, **277**, H2240-H2246.

Published on 05 February 2018. Downloaded by Fudan University on 06/02/2018 00:55:19.

Journal of Materials Chemistry B Accepted Manuscript

This journal is © The Royal Society of Chemistry 20xx

Please do not adjust margins

View Article Online
DOI: 10.1039/C7TB03200E

TOC

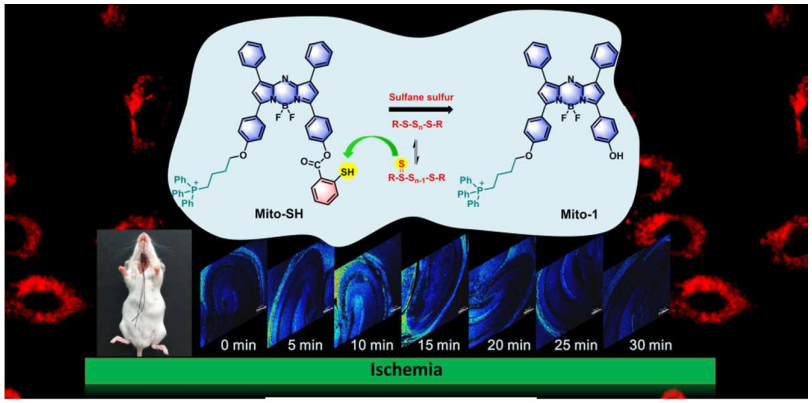

Imaging and evaluation of sulfane sulfur in acute brain ischemia using a mitochondria-targeted near-infrared fluorescent probe

Published on 05 February 2018. Downloaded by Fudan University on 06/02/2018 00:55:19.

Journal of Materials Chemistry B Accepted Manuscript